

Short Communication

A New Single Flow Zinc-Nickel Hybrid Battery Using a Ni(OH)₂-O₂ Composite cathode

Tian Wang, Meng Yang, Junqing Pan*

State Key Laboratory of Chemical Resource Engineering, Beijing University of Chemical Technology, Beijing 100029, China

*E-mail: jqpan@mail.buct.edu.cn

Received: 22 March 2017 / Accepted: 12 May 2017 / Published: 12 June 2017

A novel single flow zinc-nickel hybrid battery with a Ni(OH)₂-O₂ composite cathode was proposed. The electrolyte in this battery was a high-concentration KOH-K₂[Zn(OH)₄] solution, the anode was a copper foil electrodeposited with metallic zinc, and the cathode was the nickel hydroxide and oxygen composite electrode. High efficiencies were achieved with an average coulombic efficiency of 99.2% and an energy efficiency of 84.2% during the first 500 cycles. At the same time, no zinc dendrites accumulated on the negative electrode at the end of the discharge process. The high performance indicates that the single flow zinc-nickel battery with the new designed nickel hydroxide and oxygen composite electrode is a promising energy storage system.

Keywords: zinc-nickel hybrid battery; single flow battery; high-efficiency; hybrid structure

1. INTRODUCTION

Redox flow batteries (RFBs) are considered one of the most efficient energy storage devices and are ideal for large-scale development because of their small size and high energy storage density [1]. Since the concept of the redox flow cell was first introduced by Thaller in 1974 [2], many types of RFBs have been fabricated and developed. Examples of RFBs include zinc-bromine systems, all-vanadium systems, and polysulfide-bromine systems [3-7]. However, these redox systems require ion-exchange membranes and have a low energy density, which hinders their widespread use [8].

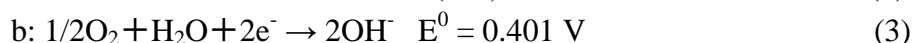
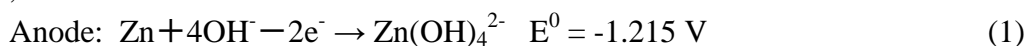
Single flow zinc-nickel (Zn-Ni(OH)₂) batteries are novel RFBs, first proposed by Cheng in 2007, and are promising energy storage systems because of their low cost (without membranes) and high energy density [9]. Although existing zinc-nickel batteries have distinct advantages, their stability

is still limited due to zinc accumulation during long-term charging and discharging cycles [10]. The increasing thickness of the negative zinc electrode ultimately causes a short circuit, which is mainly attributed to the oxygen evolution reaction at the positive electrode. Therefore, zinc accumulation is currently the most critical issue for the commercialization of zinc-nickel batteries.

Several approaches have been taken to overcome the issues mentioned above, including using new anode or cathode materials. For instance, Pan proposed a novel single flow Zn-O₂ battery in 2009 to overcome the low storage capacity of Ni(OH)₂ anode materials [11]. Additionally, a new and effective method, introduced by Zhang, improved the cycling stability by adjusting the side reactions to balance the anode and cathode reactions [12]. While the former approach has a lower energy efficiency compared to Zn-Ni(OH)₂ batteries, the latter still has side reactions at the anode or cathode.

Thus, this research focused on developing a novel single flow zinc-nickel battery with a nickel hydroxide and oxygen composite electrode, also called a zinc-nickel hybrid battery, with the following features: (i) deposited zinc was used as the anode, (ii) a new type of Ni(OH)₂ composite electrode equipped with an O₂ reduction catalyst layer was used as the cathode, (iii) and a flowing solution of KOH-K₂[Zn(OH)₄] stored in a tank and circulated using a pump was used as the electrolyte. The battery was designed to integrate the advantages of single flow Zn-Ni(OH)₂ batteries with those of novel single flow Zn-O₂ batteries. The structure of the newly designed single flow Zn-Ni(OH)₂ battery is shown in Figure 1.

When the battery is charged, Zn(OH)₄²⁻ is reduced to metallic zinc, which is electroplated onto the inert negative Cu substrate, and Ni(OH)₂ is oxidized to NiOOH at the positive electrode. At this point, there are no reactions at the O₂ electrode, and the results are shown in Figure S1. When the battery is discharged, the reverse process occurs, and highly soluble products form in the alkaline electrolyte at the zinc electrode. At the same time, residual zinc at the end of the discharge process continues to dissolve over a potential in the range of 1.2–1.4 V [11], which is consistent with single flow Zn-O₂ batteries. Eventually, the zinc electrode returns to its initial state. During the discharge process, the reactions are as follows:



The charge process is simply the reverse reaction of the discharge process, and the oxygen evolution reaction occurs at the end of the charge process.

To construct the new single flow Zn-Ni(OH)₂ batteries used in this work, α-Ni(OH)₂ microspheres and rod-shaped Ag₄Bi₂O₅ were employed as the active cathode material and the oxygen reduction catalyst, respectively. As a result, high efficiencies were achieved with an average coulombic efficiency of 99.2% and an energy efficiency of 84.2% during the first 500 cycles. Additionally, at the end of the discharge process, no zinc dendrites were accumulated on the negative electrode. The high performance of the batteries indicates that the new single flow Zn-Ni(OH)₂ hybrid battery is a feasible and promising battery.

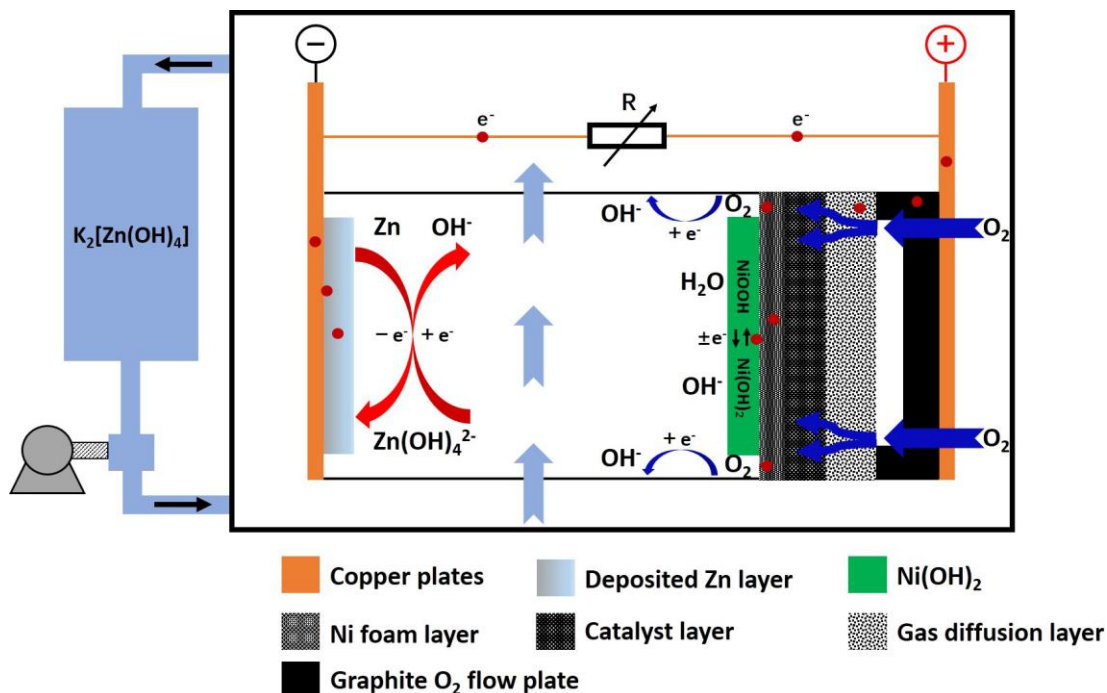


Figure 1. Illustration of the hybrid single flow Zn-Ni(OH)₂(O₂) battery.

2. EXPERIMENTAL

2.1. Materials and synthesis

All of the chemicals were of analytical grade, purchased from Beijing Fine Chemicals Co., Ltd., and used without further purification.

First, 1.2 M NiSO₄·6H₂O was dissolved in deionized water containing 0.05 M sulfuric acid and 0.02 M Na₂SO₄ to prepare the NiSO₄ mixed solution (labeled solution A). Then, 0.935 g Al(OH)₃ was dissolved in 2.4 M NaOH at 80°C (labeled solution B). Solution A and solution B were simultaneously pumped into the reactor, which contained 0.8 M of the ammonia complexing agent, at a constant velocity. The pH was maintained within 11.21-11.29, the reaction temperature was controlled at 55°C, and the stirring speed was 300 rpm. When the reaction was complete, the solution was stirred at 55°C for another 20 h, and then, the product was precipitated from solution and washed with hot deionized water until the pH of the filtered solution was neutral. Then, the product was dried under vacuum at 60°C for 4 h to obtain the α-Ni(OH)₂ product.

Rod-shaped Ag₄Bi₂O₅ was synthesized via a sedimentation method [13]. First, 1.16 g Ag₂O and 1.17 g Bi₂O₃ were dissolved in 50 mL mol L⁻¹ HNO₃ (denoted solution A). Then, 11.87 g KOH was dissolved in deionized water to obtain 50 mL of 9 mol L⁻¹ KOH (denoted solution B). Next, 50 mL of solution A and 50 mL of solution B were mixed at a flow rate of 0.2 mL min⁻¹ at a temperature of 45°C with strong agitation at 800 rpm to generate the nanosized Ag₄Bi₂O₅ sample.

2.2. Characterization

X-ray diffraction (XRD) patterns of the synthesized samples were obtained on a Rigaku D/max2500VB2+/PC diffractometer using Cu K α radiation ($\lambda = 0.15418$ nm, 40 kV, 200 mA). A field-emission scanning electron microscope (FE-SEM, Hitachi S4700) was used to characterize the morphology of the obtained samples. The amount of Zn residue in the whole battery (the bottom of the solution tank and the surface of the electrode) was measured with an inductively coupled plasma (ICP) analyzer (Agilent 7700) after dissolving in acidic solution.

2.3. Electrochemical tests

First, 0.8 g of the obtained Ni(OH) $_2$ microspheres and 0.2 g of pure expanded graphite were ground together and thoroughly mixed in an agate mortar with three drops of 60 wt.% PTFE emulsion. The obtained paste was roll-pressed into an electrode membrane with a thickness of 80 μ m for the positive electrode. An oxygen reduction catalyst layer and an oxygen-permeable membrane were proposed by our team [13]. To fabricate the positive electrode, the above materials were pressed under 10 MPa of pressure in the following order: Ni(OH) $_2$ layer - Ni foam layer - O $_2$ catalyst layer - O $_2$ - permeable membrane. The negative electrode was a piece of highly pure copper (70 \times 70 \times 0.2 mm 3). The size of the Ni(OH) $_2$ membrane was 70 \times 70 \times 0.08 mm 3 , while the Ni foam layer, the O $_2$ catalyst layer, and the O $_2$ -permeable membrane were 71 \times 71 \times 1 mm 3 , 71 \times 71 \times 0.08 mm 3 , and 71 \times 71 \times 0.1 mm 3 , respectively. The electrolyte solution was a 500 mL mixture of 8 M KOH, 20 M LiOH, and 0.7 M ZnO, which was circulated using a pump at a flow rate of 19.5 mL min $^{-1}$. Galvanostatic charge-discharge tests were carried out using a CT2000A (Jinnuo Wuhan Corp., China) battery test system at room temperature (298 K). In the charge-discharge cycles, the cell was charged at a current density of 20 mA cm $^{-2}$ (1960 mA) until a capacity of 20 mAh cm $^{-2}$ (1960 mAh) was reached, and the cell was discharged at the same current density down to a cut-off of 1.2 V.

3. RESULTS AND DISCUSSION

As seen in Figure 2a-b, the Ni(OH) $_2$ particles were composed of nano/micro-crystalline flakes, which were stacked to form a spherical nano/microstructure with a large number of loose pores on the surface. This structure facilitated the diffusion of protons and electrons and the penetration of the electrolyte. Therefore, the function of the nanoparticles is fully exerted, and the speed of the electrochemical reaction may be improved. As shown in Figure 2c and d, the Ag $_4$ Bi $_2$ O $_5$ sample had a rod-shaped crystal morphology with a width of 50-120 nm and a length of 600-1000 nm. The XRD patterns of α -Ni(OH) $_2$ and Ag $_4$ Bi $_2$ O $_5$ are shown in Figure S2 and S3, respectively. Figure S2 presents the typical diffraction peaks of the α -Ni(OH) $_2$ phase at $2\theta = 11.12^\circ$, 22.18° , 34.44° and 60.36° , corresponding to the (003), (006), (101) and (110) crystalline planes, respectively, which confirms that the product is α -Ni(OH) $_2$. For the Ag $_4$ Bi $_2$ O $_5$ sample (see Figure S3), typical peaks are observed at

31.21°, 31.78°, 37.70° and 40.498°, which correspond to the (411), (312), (600) and (420) facets of $\text{Ag}_4\text{Bi}_2\text{O}_5$ (JCPDS 87-0866), respectively.

The $\alpha\text{-Ni(OH)}_2$ microspheres were composed of ordered Ni(OH)_2 nanoflakes with enough space to permit the electrolyte to penetrate inside the spherical Ni(OH)_2 structure, which allows the electrochemical reaction to occur both inside and outside of the spherical Ni(OH)_2 particles. Moreover, the wide, layered structure was favorable for the transfer of protons and electrons, which increased the transfer speed and allowed for the generation of high current. Recently, it was found that $\text{Ag}_4\text{Bi}_2\text{O}_5$ significantly improves the discharge specific capacity and the lifespan of MnO_2 cathode materials for alkaline secondary batteries because of its enhanced catalytic activity and stability with respect to the ORR [13]. Therefore, a novel single flow zinc-nickel-oxygen battery with an even composition of 3D $\alpha\text{-Ni(OH)}_2$ and 1D $\text{Ag}_4\text{Bi}_2\text{O}_5$ should have improved electrochemical performance.

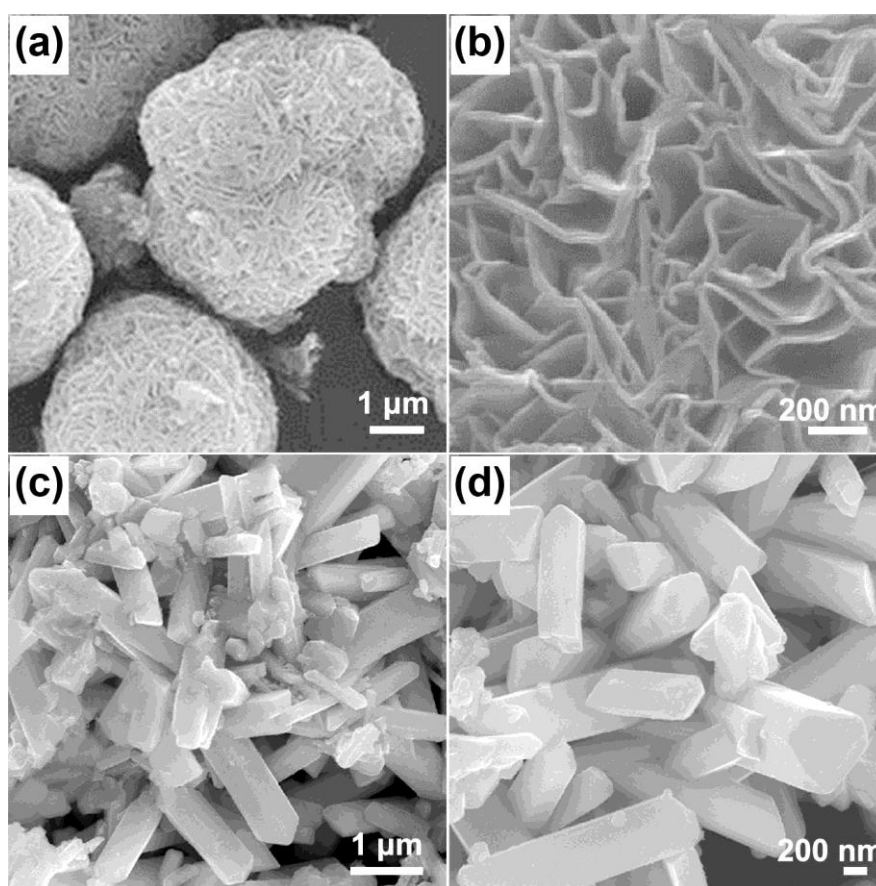


Figure 2. SEM images of (a, b) Ni(OH)_2 and (c, d) $\text{Ag}_4\text{Bi}_2\text{O}_5$ at different magnifications.

Figure 3a-b shows the charge and discharge curves of the single flow Zn- Ni(OH)_2 battery and the single flow Zn- Ni(OH)_2 hybrid battery at a charge density of 20 mA cm^{-2} for the first 500 cycles. It can be seen in Figure 3a that the electrochemical properties are stable from the 1st cycle to the 50th cycle. This battery had a discharge voltage as high as 1.63 V and a capacity of 1951.3 mAh, which was 99.6% of the charge capacity (1960 mAh). When the cycle number increased from 50 to 500, the discharge capacity decreased gradually from 1951.3 mAh to 1785.5 mAh, and the battery retained

91.5% of the initial capacity. Correspondingly, the electrochemical properties shown in Figure 3b are the same as those shown in Figure 3a from the 1st cycle to the 50th cycle, because of the activation of $\text{Ni}(\text{OH})_2$ and limited side reactions. Subsequently, although the cycle number increased, the discharge capacity remained almost constant from 1951.3 mAh at the 50th cycle to 1945.1 mAh at the 500th cycle. The battery reached 99.2% of the charge capacity (1960 mAh) and retained 99.7% of the initial capacity, which is exceptionally high.

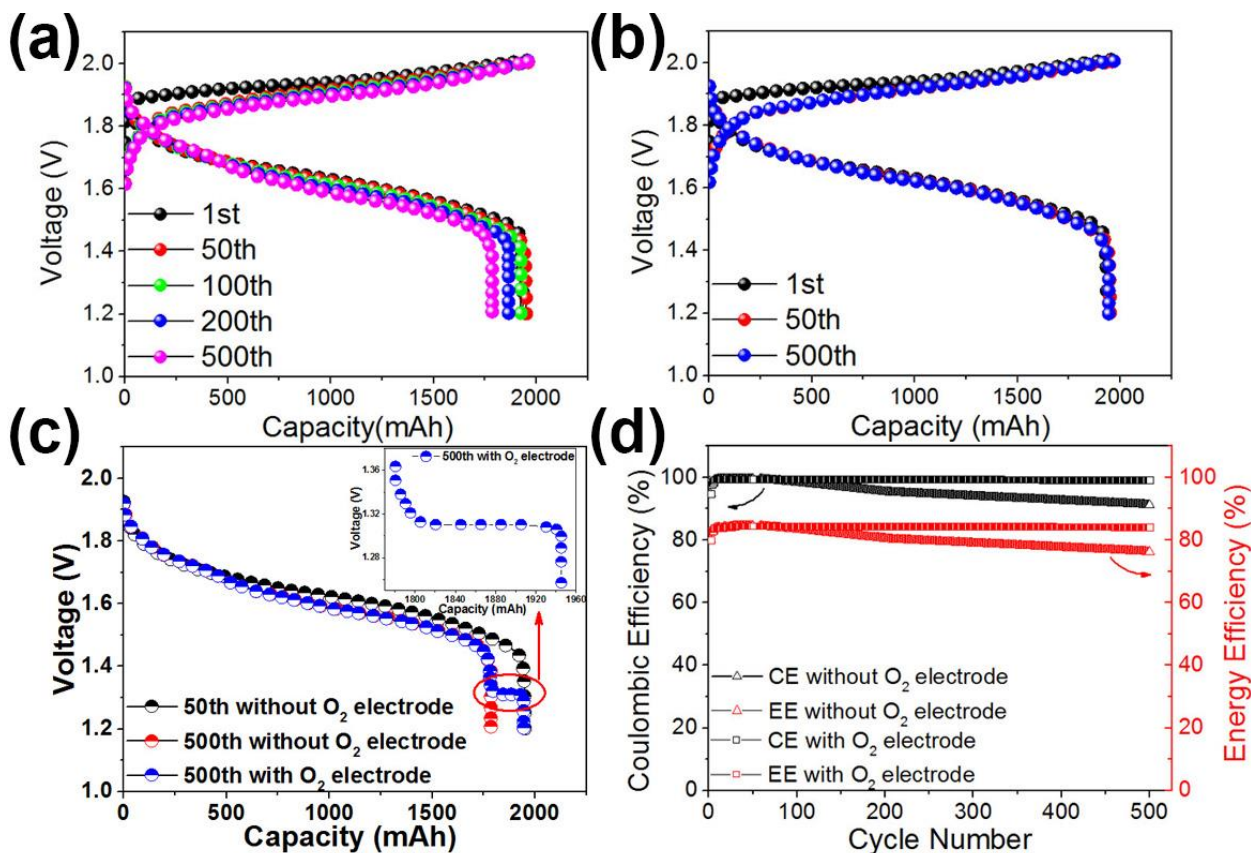


Figure 3. Charge-discharge curves of (a) the single flow Zn-Ni(OH)₂ battery and (b) the single flow Zn-Ni(OH)₂ hybrid battery. (c) Discharge curves comparing the single flow Zn-Ni(OH)₂ battery with and without the O₂ electrode at the 500th cycle, and the inset image shows the discharge curve of the single flow Zn-Ni(OH)₂ hybrid battery with O₂. (d) Coulombic efficiency and energy efficiency during 500 cycles with and without the O₂ electrode.

To gain better insight into the effects of the O₂ electrode on zinc accumulation, the discharge curves for Zn-Ni(OH)₂ with and without the O₂ electrode at the 500th cycle were compared and are shown in Figure 3c. After 500 cycles, Zn-Ni(OH)₂ was loaded with an O₂ catalyst layer in the cathode, as shown in Figure 1. It is clear that the discharge curve had two platforms at 1.60 V and 1.31 V, which correspond to the reduction of NiOOH and O₂, respectively. These results are consistent with the theoretical design at the beginning. Additionally, changes in the coulombic efficiency and energy efficiency during the charge/discharge process without and with the O₂ electrode are shown in Figure 3d. The coulombic efficiency (CE) is defined as the ratio of the discharge capacity to the charge capacity, and these values were very different for the batteries with and without the O₂ electrode. The

average values were 91.5% (without oxygen) and 99.2% (with oxygen), which implies that the O₂ electrode had an important effect on the CE of the battery. As a result, the energy efficiency (EE), which is the ratio of the discharge energy to the charge energy, increased from 76.1% (without oxygen) to 84.2% (with oxygen). As seen in the inset image in Figure 3c, the Zn-Ni(OH)₂ hybrid battery provided a small platform voltage of 1.31 V, which indicates that Zn residue is discharged by the Ni(OH)₂-oxygen electrode in air. It is helpful to dissolve the zinc residue and balance the different charge efficiencies of the two couples of Zn(OH)₄²⁻ to Zn and Ni(OH)₂ to NiOOH.

Table 1. Average quantity of accumulated zinc per cycle.

Battery	Residual zinc (mg)	Capacity (%)
Zn-Ni(OH) ₂	198.3920	8.3
Zn-Ni(OH) ₂ (O ₂)	0.0008	0.0

The ICP results of the zinc accumulated in the whole battery are shown in Table 1. The loss capacity of the battery can be calculated by Faraday's law, as follows:

$$Q = n \times z \times F = m/M \times z \times F = m/M \times 2 \times 26.8 \text{ mAh} \quad (6)$$

Herein, *m* is the mass of the accumulated zinc, *M* is the molar mass of zinc, *z* is the electron number of the reaction and *F* is Faraday's constant. The quantity of accumulated zinc decreased from 198.3920 mg (8.3% of the battery capacity) to 0.0008 mg (almost 0% of the battery charge capacity) per cycle. Figure 4 further confirms the effect of Ni(OH)₂(O₂) on the accumulated zinc. Figure 4 shows SEM images of the deposited zinc electrode in two kinds of single flow batteries after the discharge process. Obviously, there is scarcely any accumulated zinc on the surface of the electrode in the Zn-Ni(OH)₂(O₂) battery.

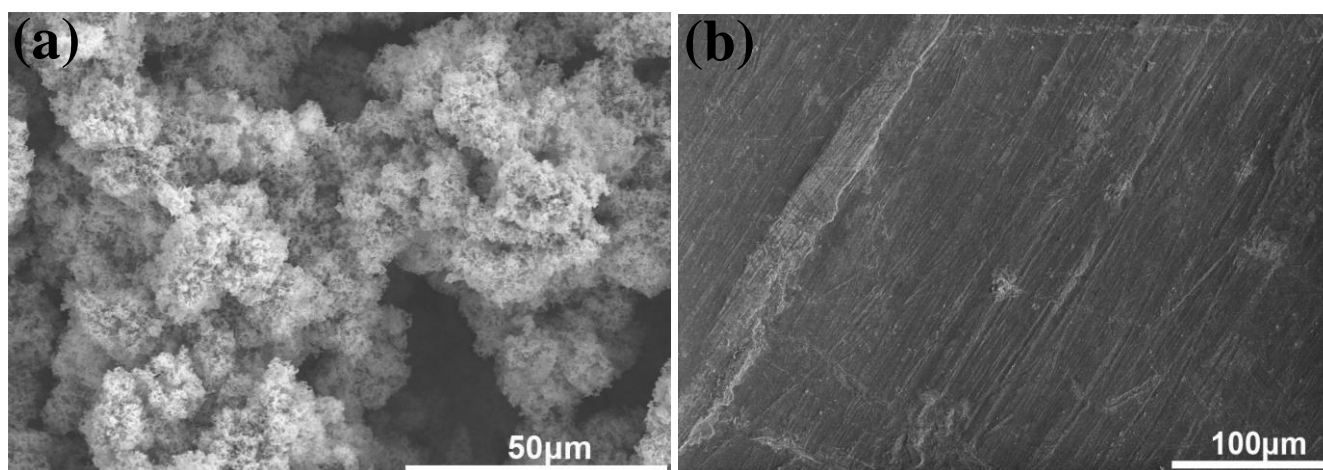


Figure 4. SEM images of the deposited zinc electrode in the (a) Zn-Ni(OH)₂ and (b) Zn-Ni(OH)₂(O₂) battery after the discharge process.

It is important to note that several recent papers have investigated the properties of single flow Zn-Ni(OH)₂ batteries. To gain better insight into the enhanced electrochemical performance of the single flow Zn-Ni(OH)₂(O₂) battery, the properties of the battery in the present work are compared

with those reported in the literature, as shown in Table 2. It can be seen that the amount of residual zinc in the Ni(OH)₂(O₂) battery is slightly higher than that in reported batteries, such as NF [12], which is mainly due to the much larger working area of the anode and cathode electrodes in this work. At the same time, both batteries show almost 0% of the respective battery charge capacity. It can also be seen that the two batteries achieve excellent cycle stability during different cycle numbers.

Table 2. Comparison of the electrochemical performances of some single flow Zn-Ni(OH)₂ batteries.

Electrode	Residual zinc (mg)	Capacity (%)	CE (%)	EE (%)	Cycle number	Reference
Nickel foam (NF)	—	—	97.3	80.1	200	[15]
Nickel foam (NF)	0.00043	0.0	96.3	78.4	400	[12]
Ni(OH) ₂	—	—	95	75.2	70	[14]
Ni(OH) ₂	—	—	96	86	1000	[9]
Ni(OH) ₂ (O ₂)	0.0008	0.0	99.2	84.2	500	This work

Furthermore, a comparison between the properties of the previously reported materials and Ni(OH)₂(O₂) is shown in Table 2. As a result, the CE and EE of Ni(OH)₂(O₂) are much higher than those of previously reported nickel-based compounds, such as Ni(OH)₂ [14,9], which indicates that the Ni(OH)₂(O₂) electrode can contribute significantly to the improvement of the CE and EE of single flow Zn-Ni(OH)₂ batteries.

All of the above results confirmed that the residual zinc was almost entirely consumed when the O₂ electrode was introduced. Therefore, the coulombic efficiency and cycling stability of the single flow Zn-Ni(OH)₂ hybrid battery was markedly improved.

4. CONCLUSIONS

A novel single flow zinc-nickel hybrid battery was reported using a nickel hydroxide/oxygen composite electrode as the cathode, electrodeposited zinc as the anode, and a concentrated solution of KOH-K₂[Zn(OH)₄] as the electrolyte. The newly designed battery showed two discharge platforms at voltages of 1.63 V and 1.31 V, with an average coulombic efficiency of 99.2% and an energy efficiency of 84.2% during the first 500 cycles. Additionally, no zinc dendrites accumulated on the negative electrode at the end of the discharge process, which indicated that the problem of zinc accumulation was successfully overcome using this method.

ACKNOWLEDGMENTS

This work was supported by National Natural Science Foundation of China (21676022), the State Key Program of National Natural Science of China (21236003), and the Fundamental Research Funds for the Central Universities (JD1701, JD1612 & YS1406).

References

1. L. Zhang, J. Cheng, Y. S. Yang, Y. H. Wen, X. D. Wang, G. P. Cao, *J. Power Sources*, 179 (2008) 381.

2. L. H. Thaller, Electrically rechargeable redox flow cell, USP: 3996064, 1974.
3. T. Yamamura, Y. Shiokawa, H. Yamana, H. Moriyama, *Electrochim. Acta*, 48 (2002) 43.
4. G. Oriji, Y. Katayama, T. Miura, *Electrochim. Acta*, 49 (2004) 3091.
5. H. T. Zhou, H. M. Zhang, P. Zhao, B. L. Yi, *Electrochim. Acta*, 51 (2006) 6304.
6. M. Skyllas-Kazacos, F. Grossmith, *J. Electrochem. Soc.*, 134 (1987) 2950.
7. P. Singh, B. Jonshagen, *J. Power Sources*, 35 (1991) 405.
8. T. Sukkar, M. Skyllas-Kazacos, *J. Membrane Sci.*, 222 (2003) 249.
9. J. Cheng, L. Zhang, Y. S. Yang, Y. H. Wen, G. P. Cao, X. D. Wang, *Electrochem. Commun.*, 9 (2007) 2639.
10. Y. H. Wen, T. Wang, J. Cheng, J. Q. Pan, G. P. Cao, Y. S. Yang, *Electrochim. Acta*, 59 (2012) 64.
11. J. Q. Pan, L. Z. Ji, Y. Z. Sun, P. Y. Wan, J. Cheng, Y. S. Yang, M. H. Fan, *Electrochem. Commun.*, 11 (2009) 2191.
12. Y. H. Cheng, Q. Z. Lai, X. F. Li, X. L. Xi, Q. Zheng, C. Ding, H. M. Zhang, *Electrochim. Acta*, 145 (2014) 109.
13. Y. Z. Sun, M. Yang, J. Q. Pan, P. Y. Wang, W. Li, P. Y. Wan, *Electrochim. Acta*, 197 (2016) 68.
14. Y. H. Cheng, H. M. Zhang, Q. Z. Lai, X. F. Li, D. Q. Shi, *Electrochim. Acta*, 105 (2013) 618.
15. Y. H. Cheng, H. M. Zhang, Q. Z. Lai, X. F. Li, D. Q. Shi, L. Q. Zhang, *J. Power Sources*, 241 (2013) 196.
16. X. H. Yue, J. Q. Pan, Y. Z. Sun, Z. H. Wang, *Ind. Eng. Chem. Res.*, 51 (2012) 8358.

© 2017 The Authors. Published by ESG (www.electrochemsci.org). This article is an open access article distributed under the terms and conditions of the Creative Commons Attribution license (<http://creativecommons.org/licenses/by/4.0/>).